Synthesis and Spectroscopic Identification of Lithium Chloro Hydride

Randell L. Mills*
Andreas Voigt
Bala Dhandapani
Jiliang He
Alejandra Echezuria

BlackLight Power, Inc.
493 Old Trenton Road
Cranbury, NJ 08512

A novel inorganic hydride compound, lithium chloro hydride (*LiHCl*), which comprises a high binding energy hydride ion was synthesized by reaction of atomic hydrogen with potassium metal and lithium chloride. Lithium chloro hydride was identified by time of flight secondary ion mass spectroscopy, X-ray photoelectron spectroscopy, ^1H nuclear magnetic resonance spectroscopy, and powder X-ray diffraction. Hydride ions with increased binding energies may form many novel compounds with broad applications such as the oxidant of a high voltage battery.

* To whom correspondence should be addressed. Phone: 609-490-1090; Fax: 609-490-1066; E-mail: rmills@blacklightpower.com

I. INTRODUCTION

It was reported previously that a new plasma source has been developed that operates by incandescently heating a hydrogen dissociator to provide atomic hydrogen and heats a catalyst such that it becomes gaseous and reacts with the atomic hydrogen to produce a plasma called a resonance transfer or rt-plasma. It was extraordinary, that intense VUV emission was observed [1-2] at low temperatures (e.g. $\approx 10^3\,K$) and an extraordinary low field strength of about 1-2 V/cm from atomic hydrogen and certain atomized elements or certain gaseous ions which singly or multiply ionize at integer multiples of the potential energy of atomic hydrogen, $27.2\,eV$. The theory has been given previously [1-8].

One such atomic catalytic system involves potassium atoms. The first, second, and third ionization energies of potassium are $4.34066\,eV$, $31.63\,eV$, and $45.806\,eV$, respectively. The triple ionization ($t=3$) reaction of K to K^{3+}, then, has a net enthalpy of reaction of $81.7766\,eV$, which is equivalent to $3\cdot 27.2\,eV$. It has been reported [8] that an rt-plasma was observed from incandescently heated atomic hydrogen and the atomized potassium catalyst. No plasma or VUV emission was observed with potassium or hydrogen alone or when sodium replaced potassium with hydrogen. Emission was observed from K^{3+} that confirmed the resonant nonradiative energy transfer of $3\cdot 27.2\,eV$ from atomic hydrogen to atomic potassium. The catalysis reaction products are novel hydrides. The predicted hydride ion of hydrogen catalysis by atomic potassium is the hydride ion $H^-(1/4)$ [8]. This ion was reported to be been observed spectroscopically at $110\,nm$ corresponding to its predicted binding energy of $11.2\,eV$ [8].

Hydride ions with high binding energies have been observed by XPS and by solid state magic-angle spinning proton nuclear magnetic resonance (^1H MAS NMR) having upfield shifted peaks [4-7]. Additional prior related studies that support the possibility of a novel reaction of atomic hydrogen which produces a chemically generated or assisted plasma (rt-plasma) and produces novel hydride compounds include extreme ultraviolet (EUV) spectroscopy [1-3, 8-13], characteristic emission from catalysis and the hydride

ion products [8-9], emission of hydrogen intermediates [3], plasma formation [1-2, 8-11], Balmer α line broadening [2-3, 10, 12-13], elevated electron temperature [3, 12-13], anomalous plasma afterglow duration [11], power generation [3, 12], and analysis of chemical compounds [4-7]. In prior reports [4-7], novel inorganic alkali and alkaline earth hydrides of the formula *MHX* and *MHMX* wherein *M* is the metal, *X*, is a singly negatively charged anion, and *H* comprises a novel high binding energy hydride ion were synthesized in a high temperature gas cell by reaction of atomic hydrogen with a catalyst and *MX* or MX_2 corresponding to an alkali metal or alkaline earth metal, respectively. We report on the synthesis and spectroscopic identification of *LiHCl* which is a new compound of this series.

EXPERIMENTAL

Synthesis

Lithium chloro hydride, *LiHCl*, was prepared in a stainless steel gas cell shown in Figure 1 comprising a Ni screen hydrogen dissociator (Belleville Wire Cloth Co., Inc.), potassium metal catalyst (Aldrich Chemical Company), and *LiCl* (Aldrich Chemical Company 99.9 %) as the reactant. A 304-stainless steel cell was in the form of a tube having an internal cavity of 359 millimeters in length and 73 millimeters in diameter. The top end of the cell was welded to a high vacuum 4 5/8 inch bored through conflat flange. The mating blank conflat flange contained a single coaxial hole in which was welded a 3/8 inch diameter stainless steel tube that was 100 cm in length and contained an inner coaxial tube of 1/8 inch diameter. A silver plated copper gasket was placed between the two flanges. The two flanges were held together with 10 circumferential bolts. The bottom of the 3/8 inch tube was flush with the bottom surface of the top flange. The outer tube served as a vacuum line from the cell and the inner tube served as a hydrogen or helium supply line to the cell. The cell was surrounded by four heaters. Concentric to the heaters was high temperature insulation (AL 30 Zircar). Each of the four heaters were individually thermostatically controlled.

The cylindrical wall of the cell was lined with two layers of Ni screen totaling 150 grams. 3 grams of crystalline *LiCl* was poured into the cell. About 0.5 grams of potassium metal was added to the cell under an argon atmosphere. The cell was then continuously evacuated with a high vacuum turbo pump to reach 50 mTorr measured by a pressure gauge (Varian Convector, Pirrani type). The cell was heated by supplying power to the heaters. The heater power of the largest heater was measured using a wattmeter (Clarke -Hess model 259). The temperature of the cell was measured with a type K thermocouple (Omega). The cell temperature was then slowly increased over 2 hours to 300 °C using the heaters that were controlled by a type 97000 controller. The power to the largest heater and the cell temperature and pressure were continuously recorded by a DAS. The vacuum pump valve was closed. Hydrogen was slowly added to maintain a pressure within the range of 1000 Torr to 1500 Torr. The temperature of the cell was then slowly increased to 550 °C over 5 hours. The hydrogen valve was closed except to maintain the pressure at 1500 Torr. After 72 hours, the temperature of the cell was reduced to 400 °C at a rate of 15 °C/hr. The hydrogen supply was switched to helium which was flowed through the inner supply line to the cell while a vacuum was pulled on the outer vacuum line to remove volatilized potassium metal at 400 °C. The cell was then cooled and opened. About 3 grams of light green/brown crystals were observed to have formed in the bottom of the cell.

ToF-SIMS Characterization

The crystalline samples were grounded into powder in a drybox, and then sprinkled onto the surface of a double-sided adhesive tape and characterized using Physical Electronics TRIFT ToF-SIMS instrument. The primary ion source was a pulsed $^{69}Ga^{+}$ liquid metal source operated at 15 keV. The secondary ions were exacted by a ± 3 keV (according to the mode) voltage. Three electrostatic analyzers (Triple-Focusing-Time-of-Flight) deflect them in order to compensate for the initial energy dispersion of ions of the same mass. The 400 pA dc current was pulsed at a 5 kHz repetition

rate with a 7 ns pulse width. The analyzed area was $60\mu m$ x $60\mu m$ and the mass range was 0-1000 AMU. The total ion dose was $7 X 10^{11}$ $ions/cm^2$, ensuring static conditions. Charge compensation was performed with a pulsed electron gun operated at 20 eV electron energy. In order to remove surface contaminants and expose a fresh surface for analysis, the samples were sputter-cleaned for 30 s using a $80\mu m$ x $80\mu m$ raster, with 600 pA current, resulting in a total ion dose of 10^{15} $ions/cm^2$. Three different regions on each sample of $60\mu m$ x $60\mu m$ were analyzed. The positive and negative SIMS spectra were acquired. Representative post sputtering data is reported. The ToF-SIMS data were treated using 'cadence' software (Physical Electronics), which calculates the mass calibration from well-defined reference peaks.

XPS Characterization

A series of XPS analyses of low binding energy region (0 to 100 eV) were made on the crystalline samples using a Scienta 300 XPS Spectrometer. The fixed analyzer transmission mode and the sweep acquisition mode were used. The step energy in the survey scan was $0.5\,eV$, and the step energy in the high resolution scan was $0.15\,eV$. In the survey scan, the time per step was 0.4 seconds, and the number of sweeps was 4. In the high resolution scan, the time per step was 0.3 seconds, and the number of sweeps was 30. $C\,1s$ at $284.5\,eV$ was used as the internal standard.

The binding energies and features of core level electrons of control *LiCl* and the crystals comprising the *LiHCl* sample were analyzed by a Kratos XSAM-800 spectrometer using nonmonochromatic $Al\,K\alpha$ (1468.6 eV) radiation. Samples were crushed in a glove box under argon and mounted on an analysis stub with copper tape. A piece of gold foil was stuck into the sample for calibration. The samples were transferred from glove box to sample treatment chamber under an inert atmosphere. A survey spectrum was run from 1000 eV to 0 eV. For quantitative analysis, high resolution spectra were run on core level electrons of interest, *Li* 1s and *Cl* 2p electrons. A high resolution spectrum of the low binding energy region was also run from 120 eV to 0 eV that corresponded

to the survey spectrum. Fixed analyzer transmission (FAT) mode was used in all measurements. For the survey scan, a pass energy of 320 eV was employed. A pass energy of 40 eV was used for high resolution scans. In the cases where a charging effect was observed, the spectrum was corrected by using a calibration of $Au\,4f_{7/2}$ peak at 84.0 eV as a first standard and the $C\,1s$ peak at 284.5 eV as a second standard.

NMR Spectroscopy

Solid state ^1H MAS NMR was performed on the samples using a custom built spectrometer operating with a Nicolet 1280 computer. Final pulse generation was from a tuned Henry radio amplifier. The ^1H NMR frequency was 270.6196 MHz. A 5 μsec pulse corresponding to a 41° pulse length and a 3 second recycle delay were used. The window was $\pm 20\,kHz$. The spin speed was 4.0 kHz. The number of scans was 600. The offset was 1541.6 Hz, and the magnetic flux was 6.357 T. The samples were handled under a nitrogen atmosphere. Chemical shifts were referenced to external tetramethylsilane (TMS). The reference comprised *LiH* (Aldrich Chemical Company 99%) and equivalent molar mixtures of *LiH* (Aldrich Chemical Company 99%) and *LiCl* (Aldrich Chemical Company 99.99%) prepared in a glove box under argon.

Characterization by X-ray Diffraction (XRD)

The XRD patterns were obtained by IC Laboratories (Amawalk, NY) using a Phillips 547 Diffractometer tuned for $Cu\,K_\alpha$ (1.540590 Å) radiation generated at 45 kV and 35 mA. The sample was scanned from 8 to 68 2-theta with a step size of 0.02° and 1 second per step.

RESULTS

ToF-SIMS

The positive ToF-SIMS spectra obtained from *LiHCl* and *LiCl* control are shown in Figures 2 and 3, respectively. The positive ion spectrum of *LiHCl* and that of the *LiCl* were dominated by the Li^+ ion. Ga^+ $m/z=69$, K_2^+ $m/z=78$, K_2H^+ $m/z=79$, K_2O^+ $m/z=94$, K_2OH^+ $m/z=95$, $K(KCl)^+$ $m/z=113$, KCO_3^+ $m/z=122$, $KHCO_3^+$ $m/z=123$

and $K_3CO_3^+$ $m/z = 177$ were also observed in the *LiHCl* sample. The presence of K in the *LiHCl* sample was due to the addition of K metal as a catalyst in the synthesis of *LiHCl*.

The negative ion ToF-SIMS of the *LiHCl* shown in Figure 4 was dominated by H^-, O^- and Cl^- peaks. Oxygen contamination was from some air exposure during sample preparation. The Cl^- count was lower than H^-; whereas, Cl^- dominated the negative ion ToF-SIMS of the *LiCl* control shown in Figure 5. H^- $m/z = 1$, and O^- $m/z = 16$, were also observed in *LiCl*.

XPS

A survey spectrum was obtained over the region $E_b = 0\ eV$ to $1200\ eV$. The primary element peaks allowed for the determination of all of the elements present in the *LiHCl* and the control *LiCl*. The survey spectrum also detected shifts in the binding energies of the elements which had implications to the identity of the compound containing the elements.

The major species present in control *LiCl* were lithium and chlorine. The XPS survey scan of the *LiHCl* sample obtained on the Scienta instrument is shown in Figure 6. Potassium and oxygen from air exposure of the potassium catalyst during sample preparation was present as well as lithium. Chlorine was observed in the low binding energy region.

The 0-120 eV binding energy region of high resolution XPS spectra of the *LiHCl* sample (solid), the control *LiCl* (dashed), and the 0-30 eV region of an additional control *KCl* obtained on the Scienta instrument are shown in Figure 7. Elements present in the survey scan which could be assigned to peaks in the low binding energy region of the *LiHCl* sample were the *K 3p* and *K 3s* peaks at 19 eV and 35 eV, respectively, the *O 2s* at 24 eV, *Li* 1s at 55 eV, and the *Cl* 3p peak at 6.5 eV. Accordingly, any other peaks in this region must be due to novel species. The XPS spectrum of the *LiHCl* sample differs from those of *LiCl* and *KCl* by having additional features at 11.2 eV and 14.7 eV. *LiOH* was present in *LiCl* and the *LiHCl* sample as shown by the presence of *O 2s* in Figure 7. Thus, the novel peaks can not be assigned to *LiOH*.

The 0-120 eV binding energy region of high resolution XPS spectra of the *LiHCl* sample (solid) and the control *LiCl* (dashed) obtained on the Scienta instrument is shown in Figure 8. Hydrogen is the only element which does not have primary element peaks; thus, it is the only candidate to produce the novel peaks. The XPS peaks centered at 11.2 eV and 14.7 eV that do not correspond to any other primary element peaks may correspond to the $H^-(n=1/4)\,E_b=11.2\,eV$ hydride ion shown previously [8] in two different chemical environments where E_b is the predicted vacuum binding energy. Figure 8 also shows that the *Li* 1s peak of *LiHCl* was shifted about 1.7 eV to lower binding energies relative to the *Li* 1s peak of *LiCl* possibly due to the presence of $H^-(n=1/4)$.

The binding energies and features of core level electrons of control *LiCl* and the *LiHCl* sample were analyzed by XPS. The local structure of *LiCl* and the *LiHCl* sample was investigated by studying the metal *Li* 1s core level electrons and the chloride *Cl* 2p core level electrons. As atomic hydrogen undergoes reaction with potassium catalyst to form a lower-energy hydrogen species which subsequently reacts with the lithium center in *LiCl*, alterations in the electronic structure of lithium such as changes in core level binding energies relative to the starting compound, *LiCl*, were expected.

The XPS spectra of the *Li* 1s core level in *LiCl* and *LiHCl* appear in Figures 9A and 9B respectively. The *Li* 1s binding energy (54.96 eV) in the *LiHCl* sample is about 1.7 eV lower than that of *Li* 1s (56.66 eV) in the control *LiCl*. The full width at half maximum (FWHM) in *Li* 1s from the *LiHCl* sample is about 0.17 eV broader than that from control *LiCl*. The presence of the novel hydride ion shifted the *Li* 1s peaks to lower binding energies relative to the corresponding peaks of *LiCl*. A similar shift in the *Li* 1s core level of the *LiHCl* sample was observed when compared to *Li* 1s of *LiCl* recorded with the Scienta instrument as shown in Figure 8.

The XPS spectra of the *Cl* 2p core level in *LiCl* and *LiHCl* appear in Figures 10A and 10B respectively. In contrast to the *Li* 1s core level, the *Cl* 2p core level FWHM in the *LiHCl* sample is very similar to *LiCl*. Comparing the alterations in the *Li* core level versus the *Cl* core level indicates that the lower-energy hydrogen species is bound

to the metal center of *LiCl*. This binding largely influences the metal core level with little perturbation of the halogen core level.

The XPS data clearly indicates a change in the electronic structure at the *Li* core level and different bonding in *LiHCl* relative to that in the corresponding *LiCl*. It strongly suggests the formation of a novel metal hydride which is consistent with the supporting data provided by XPS given above, NMR and ToF-SIMS given in the respective sections.

The XPS survey scans of *LiCl* and the *LiHCl* sample obtained on the Kratos instrument are shown in Figures 11A-B, respectively. The 0-100 eV binding energy region of high resolution XPS spectra of *LiCl* and the *LiHCl* sample obtained on the Kratos instrument are shown in Figures 12A-B, respectively. Hydrogen is the only element which does not have primary element peaks; thus, it is the only candidate to produce the shifted *Li* 1s peak of the *LiHCl* sample compared to *LiCl* as shown in Figures 12A-B.

NMR

The ^{1}H MAS NMR spectra of the *LiHCl* sample, the control comprising an equal molar mixture of *LiH* and *LiCl*, and the control *LiH* relative to external tetramethylsilane (TMS) are shown in Figures 13A-C, respectively. Ordinary hydride ion has resonances at 4.2 ppm and 1.1 ppm in the *LiH/ LiCl* mixture and in *LiH* alone as shown in Figures 13B and 13C, respectively. The presence of *LiCl* does not shift the resonance of ordinary hydride as shown in Figure 13B. The resonance at 4.2 ppm and 1.2 ppm which are assigned to ordinary hydride ion was observed in the spectrum of the *LiHCl* sample as shown in Figure 13A. A large distinct upfield resonance was observed at -15.2 ppm, and features were observed at -1.7 ppm and -9 ppm. These features were not observed in either control. The upfield shifted peaks are consistent with a hydride ion with a smaller radius as compared with ordinary hydride since a smaller radius increases the shielding or diamagnetism. This upfield shifted peak was assigned to a novel hydride ion of *LiHCl* in different chemical environments. The down field shifted peak at 13.3 ppm may have been due to H^{+} stabilized by the novel H^{-}.

XRD

The XRD pattern of *LiHCl* is shown in Figure 14. The identifiable peaks corresponded to a mixture of *LiH*, *LiO* and *LiOH*. In addition, the spectrum contained a number of peaks that could not be assigned. The 2-theta and d-spacings of the unidentified XRD peaks of the *LiHCl* sample are given in Table 1.

DISCUSSION

The ToF-SIMS of the product of the reaction of atomic hydrogen with potassium metal and *LiCl* showed Li^+ and H^- as the dominant peaks with Cl^- present. The potassium metal was oxidized by air exposure during sample preparation. The ToF-SIMS results recorded on the reaction product are consistent with the proposed structure *LiHCl*. The NMR and XPS data indicate that a novel hydride ion was present. The known compounds *LiCl* and *LiH* have the lithium ion in a +1 state. The compound *LiHCl* is unknown and extraordinary. The implied valence of lithium is +2.

The 0-100 eV binding energy region of a high resolution XPS spectrum of the *LiHCl* sample indicates the presence of the hydride ion $H^-(1/4)$ with binding energies of 11.2 eV and 14.7 eV compared to the predicted binding energy of 11.2 eV. The presence of two peaks may have been due to the presence $H^-(1/4)$ in two different chemical environments. The XPS data of the core levels clearly indicates a change in the electronic structure and different bonding in *LiHCl* relative to that in the corresponding *LiCl*. This binding influences the metal core level with little perturbation of the halogen core level. Comparing the alterations in the *Li* core levels versus the *Cl* core level indicates that the lower-energy hydrogen species binds to the metal center of *LiCl*. The presence of the novel hydride ion shifts the *Li* 1s peaks to lower binding energies relative to the corresponding peaks of *LiCl*. It strongly suggests the formation of a novel metal hydride which is consistent with the supporting data provided by XPS , NMR and ToF-SIMS.

The resonances in the NMR spectrum of the *LiHCl* at 4.2 ppm and 1.1 ppm were assigned to ordinary hydride ion. The large distinct upfield resonance at -15.2 ppm, and features observed at -1.7 ppm and -9 ppm identifies a hydride ion with a substantially smaller radius as compared with ordinary hydride since a smaller radius increases the shielding or diamagnetism, and the shift was extraordinary. *LiHCl* was possibly present in different chemical environments as evidenced by the three distinct upfield shifts.

XRD peaks were observed which did not match those known which supported the identification of a novel compound.

CONCLUSIONS

LiHCl was synthesized by reaction of atomic hydrogen with potassium catalyst in the presence of *LiCl*. The ToF-SIMS, XPS, and NMR results supported the identification of *LiHCl* comprising a hydride having a high binding energy of 11.2 eV that matched prior theoretical predictions [8]. The identification of compounds containing novel hydrides is indicative of a new area of hydride chemistry with the potential for significant applications. For example, a high voltage battery according to the hydride binding energies in *LiHCl* and previously observed by XPS [5-7, 14] may be possible having projected specifications that are significantly exceed those of the current state of the art [6, 15].

REFERENCES

1. R. Mills, J. Dong, Y. Lu, "Observation of Extreme Ultraviolet Hydrogen Emission from Incandescently Heated Hydrogen Gas with Certain Catalysts", Int. J. Hydrogen Energy, Vol. 25, (2000), pp. 919-943.
2. R. Mills and M. Nansteel, P. Ray, "Argon-Hydrogen-Strontium Discharge Light Source", IEEE Transactions on Plasma Science, in press.
3. R. L. Mills, P. Ray, B. Dhandapani, M. Nansteel, X. Chen, J. He, "Spectroscopic Identification of Transitions of Fractional Rydberg

States of Atomic Hydrogen", J. of Quantitative Spectroscopy and Radiative Transfer, in press.

4. R. Mills, B. Dhandapani, M. Nansteel, J. He, A. Voigt, "Identification of Compounds Containing Novel Hydride Ions by Nuclear Magnetic Resonance Spectroscopy", Int. J. Hydrogen Energy, Vol. 26, No. 9, Sept. (2001), pp. 965-979.
5. R. Mills, B. Dhandapani, N. Greenig, J. He, "Synthesis and Characterization of Potassium Iodo Hydride", Int. J. of Hydrogen Energy, Vol. 25, Issue 12, December, (2000), pp. 1185-1203.
6. R. Mills, "Novel Inorganic Hydride", Int. J. of Hydrogen Energy, Vol. 25, (2000), pp. 669-683.
7. R. Mills, B. Dhandapani, M. Nansteel, J. He, T. Shannon, A. Echezuria, "Synthesis and Characterization of Novel Hydride Compounds", Int. J. of Hydrogen Energy, Vol. 26, No. 4, (2001), pp. 339-367.
8. R. Mills, P. Ray, Spectroscopic Identification of a Novel Catalytic Reaction of Potassium and Atomic Hydrogen and the Hydride Ion Product, Int. J. Hydrogen Energy, Vol. 27, No. 2, February, (2002), pp. 183-192.
9. R. Mills, "Spectroscopic Identification of a Novel Catalytic Reaction of Atomic Hydrogen and the Hydride Ion Product", Int. J. Hydrogen Energy, Vol. 26, No. 10, (2001), pp. 1041-1058.
10. R. L. Mills, P. Ray, "A Comprehensive Study of Spectra of the Bound-Free Hyperfine Levels of Novel Hydride Ion $H^-(1/2)$, Hydrogen, Nitrogen, and Air", Int. J. Hydrogen Energy, in press.
11. R. Mills, T. Onuma, and Y. Lu, "Formation of a Hydrogen Plasma from an Incandescently Heated Hydrogen-Catalyst Gas Mixture with an Anomalous Afterglow Duration", Int. J. Hydrogen Energy, Vol. 26, No. 7, July, (2001), pp. 749-762.
12. R. L. Mills, P. Ray, "Substantial Changes in the Characteristics of a Microwave Plasma Due to Combining Argon and Hydrogen", New Journal of Physics, www.njp.org, Vol. 4, (2002), pp. 22.1-22.17.
13. R. L. Mills, P. Ray, B. Dhandapani, J. He, "Comparison of Excessive Balmer α Line Broadening of Glow Discharge and Microwave Hydrogen Plasmas with Certain Catalysts", J. of Applied Physics, submitted.

14. R. L. Mills, B. Dhandapani, J. He, "Highly Stable Amorphous Silicon Hydride", J of Materials Research, submitted.
15. R. L. Mills, E. Dayalan, "Novel Alkali and Alkaline Earth Hydrides for High Voltage and High Energy Density Batteries", Proceedings of the 17th Annual Battery Conference on Applications and Advances, California State University, Long Beach, CA, (January 15-18, 2002), in press.

Table 1. The 2-theta and d-spacings of the unidentified XRD peaks of the *LiHCl* sample.

Peak Number	2 – Theta (Deg)	d (Å)
2	26.60	3.3518
3	26.96	3.3066
4	30.70	2.9128
11	45.71	1.9849
12	49.26	1.8497
16	62.21	1.4923

Figure Captions

Figure 1. Stainless steel gas cell.

Figure 2. The positive ToF-SIMS spectrum ($m/e = 0-200$) of the *LiHCl* sample that shows Li^+ as the dominate positive ion.

Figure 3. The positive ToF-SIMS spectrum ($m/e = 0-200$) of *LiCl* that shows Li^+ as the dominate positive ion.

Figure 4. The negative ToF-SIMS spectrum ($m/e = 0-200$) of the *LiHCl* sample that shows H^- as the dominate negative ion.

Figure 5. The negative ToF-SIMS spectrum ($m/e = 0-200$) of *LiCl* that shows Cl^- as the dominate negative ion.

Figure 6. The XPS survey scan of the *LiHCl* sample obtained on the Scienta instrument that shows the presence of potassium and oxygen from air exposure of the potassium catalyst during sample preparation as well as lithium.

Figure 7. The 0-120 eV binding energy region of high resolution XPS spectra of the *LiHCl* sample (solid), the control *LiCl* (dashed), and the 0-30 eV region of an additional control *KCl* obtained on the Scienta instrument. The XPS peaks centered at 11.2 eV and 14.7 eV can not be assigned to *LiCl*, *KCl*, or *LiOH*.

Figure 8. The 0-120 eV binding energy region of high resolution XPS spectra of the *LiHCl* sample (solid) and the control *LiCl* (dashed) obtained on the Scienta instrument. The XPS peaks centered at 11.2 eV and 14.7 eV that do not correspond to any other primary element peaks may correspond to the $H^-(n=1/4)\,E_b = 11.2\,eV$ possibly in two different chemical environments where E_b is the predicted vacuum binding energy. The *Li* 1s peak of *LiHCl* is shifted about 1.7 eV to lower binding energies relative to the *Li* 1s peak of *LiCl* possibly due to the presence of $H^-(n=1/4)$.

Figure 9A. The XPS spectrum of the *Li* 1*s* core level in *LiCl* obtained on the Kratos instrument.

Figure 9B. The XPS spectrum of the *Li* 1*s* core level in *LiHCl* obtained on the Kratos instrument. The *Li* 1s binding energy (54.96 eV) in the *LiHCl* sample is about 1.7 eV lower than that of *Li* 1s (56.66 eV) in the control *LiCl*. The full width at half maximum (FWHM) in *Li* 1s from the *LiHCl* sample is about 0.17 eV broader than that from control *LiCl*.

Figure 10A. The XPS spectrum of the *Cl 2p* core level in *LiCl* obtained on the Kratos instrument.

Figure 10B. The XPS spectrum of the *Cl 2p* core level in *LiHCl* obtained on the Kratos instrument.

Figure 11A. The XPS survey scan of *LiCl* obtained on the Kratos instrument.

Figure 11B. The XPS survey scan of the *LiHCl* sample obtained on the Kratos instrument. The *Cl* 2p core level FWHM in the *LiHCl* sample is very similar to that of *LiCl*.

Figure 12A. The 0-100 eV binding energy region of a high resolution XPS spectrum of *LiCl* obtained on the Kratos instrument.

Figure 12B. The 0-100 eV binding energy region of a high resolution XPS spectrum of the *LiHCl* sample obtained on the Kratos instrument. Hydrogen is the only element which does not have primary element peaks; thus, it is the only candidate to produce the shifted *Li* 1s peak.

Figure 13A. The ^{1}H MAS NMR spectrum of *LiHCl* relative to external tetramethylsilane (TMS). The resonances at 4.2 ppm and 1.1 ppm were assigned to ordinary hydride ion. The large distinct upfield resonance at -15.2 ppm, and features observed at -1.7 ppm and -9 ppm identified a hydride ion with a substantially smaller radius as compared with ordinary hydride since a smaller radius increases the shielding or diamagnetism. The upfield peaks were assigned to a novel hydride ion of *LiHCl* possibly in different chemical environments.

Figure 13B. The ^{1}H MAS NMR spectrum of the control comprising an equal molar mixture of *LiH* and *LiCl* relative to external tetramethylsilane (TMS). Ordinary hydride ion has resonances at 4.2 ppm and 1.1 ppm in the *LiH/ LiCl* mixture and in *LiH*. The presence of *LiCl* does not shift the resonance of ordinary hydride as shown in Figure 13C.

Figure 13C. The ^{1}H MAS NMR spectrum of the control *LiH* relative to external tetramethylsilane (TMS).

Figure 14. The X-ray Diffraction (XRD) pattern of the *LiHCl* sample. Unidentified XRD peaks of *LiHCl* are given in Table 1.

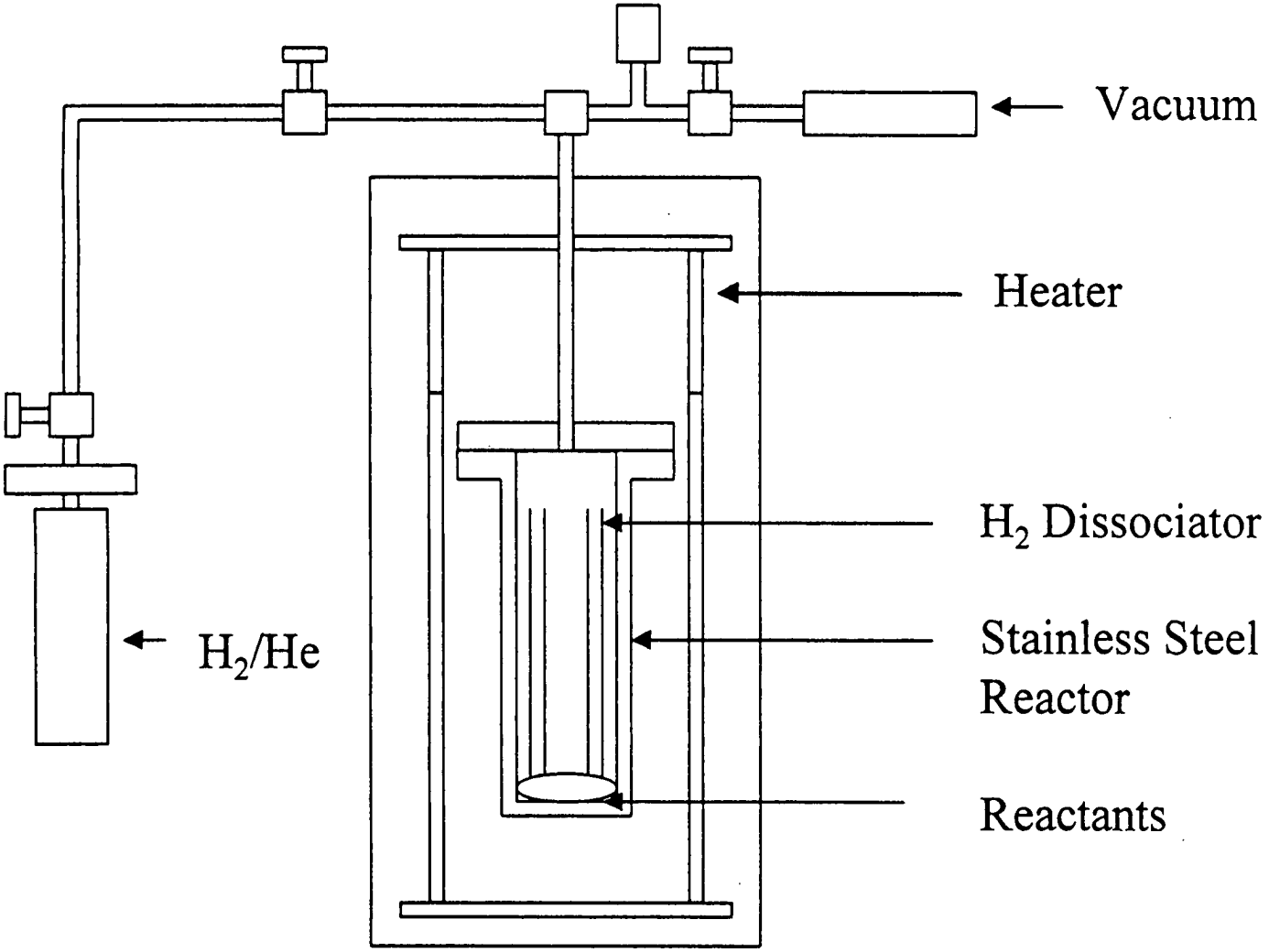
Vacuum
Heater
H_2 Dissociator
Stainless Steel Reactor
Reactants
H_2/He

Fig. 1

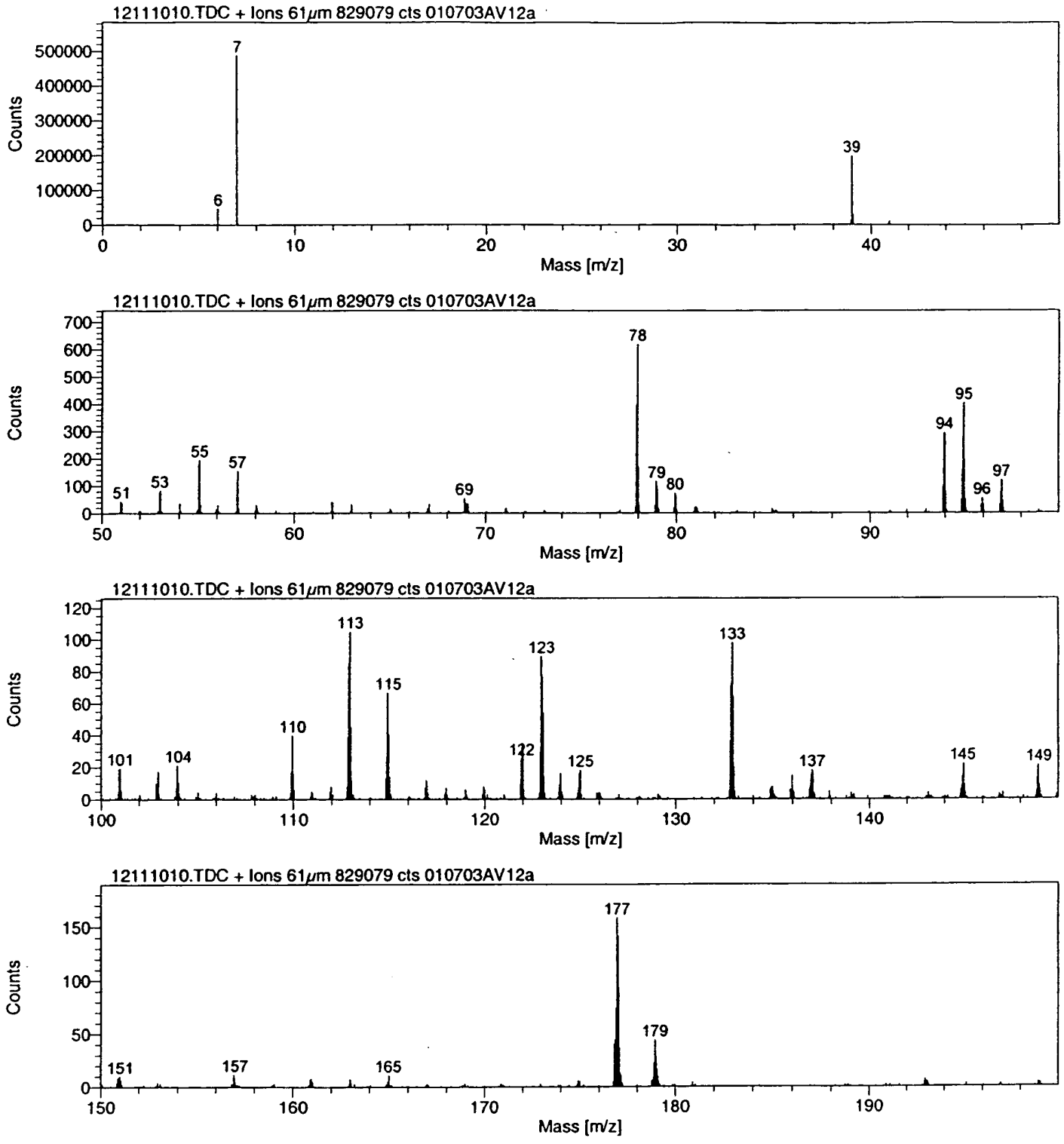
12111010.TDC + Ions 61μm 829079 cts 010703AV12a
Counts
Mass [m/z]
7
6
39
78
95
94
55
57
53
51
69
79
80
97
96
113
123
133
115
110
101
104
122
125
137
145
149
177
179
151
157
165

Fig. 2

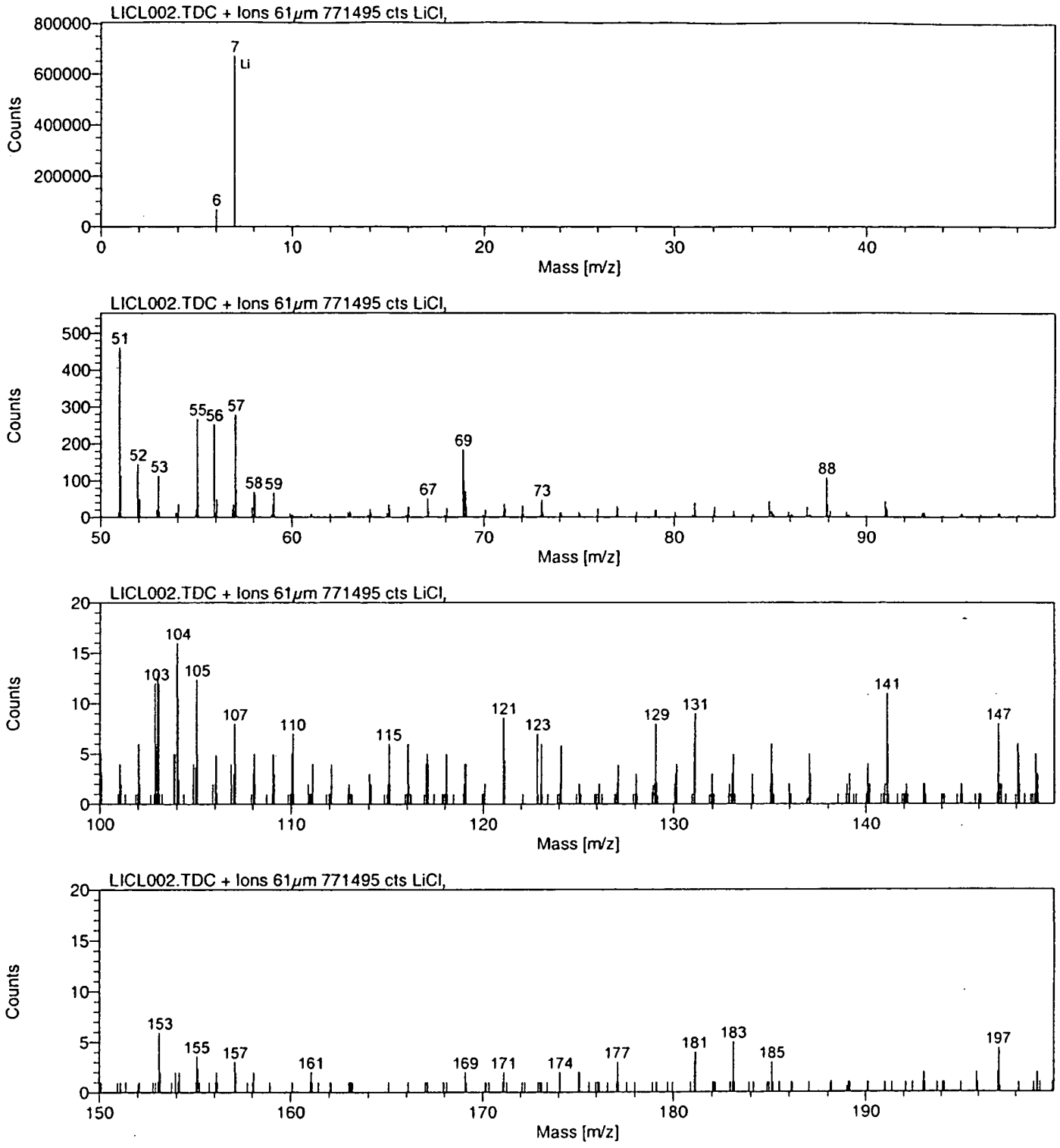
LICL002.TDC + Ions 61μm 771495 cts LiCl,
Counts
Mass [m/z]
7
Li
6
51
52
53
55
56
57
58
59
67
69
73
88
104
103
105
107
110
115
121
123
129
131
141
147
153
155
157
161
169
171
174
177
181
183
185
197

Fig. 3

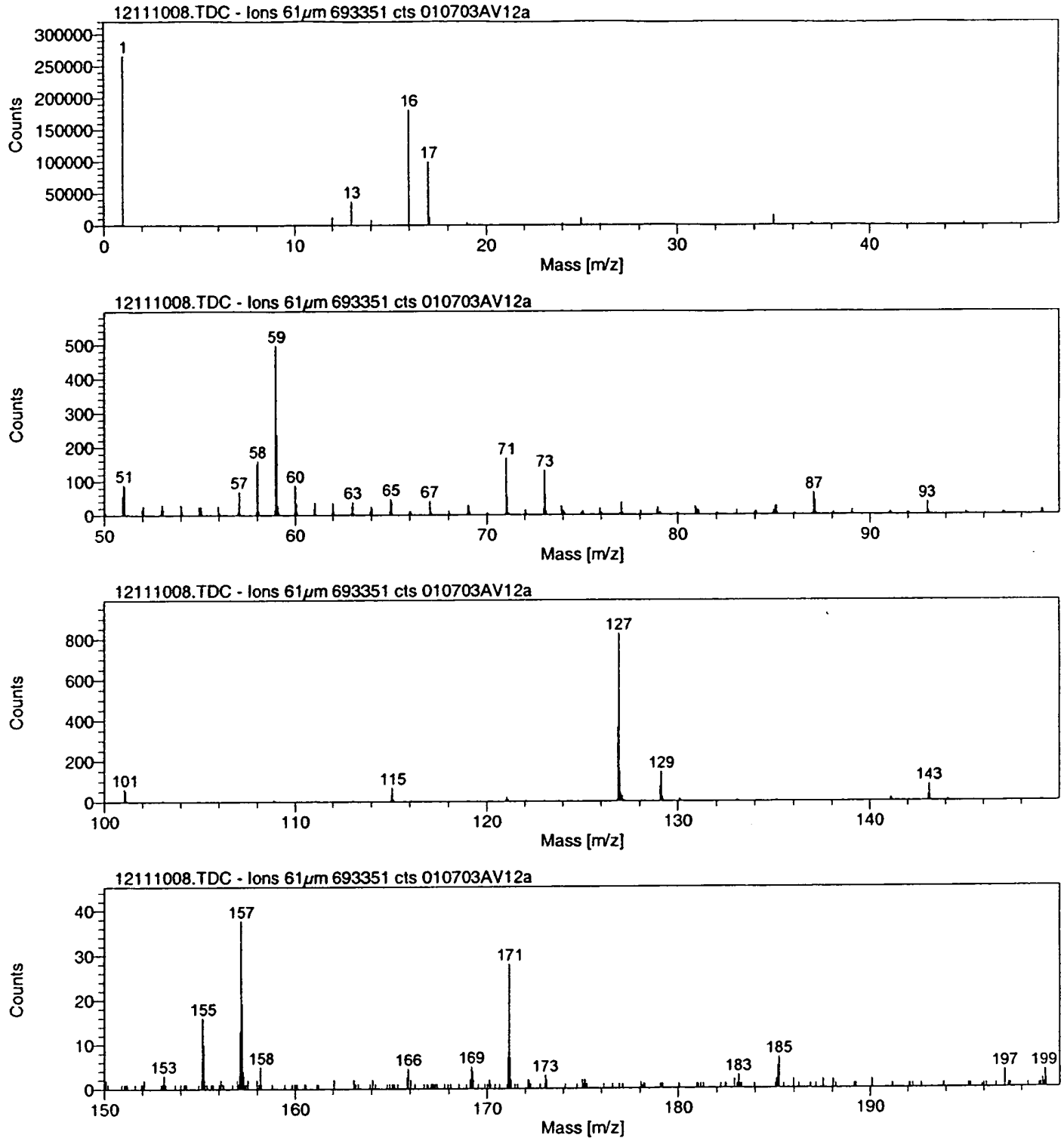
12111008.TDC - Ions 61μm 693351 cts 010703AV12a
Counts
Mass [m/z]
1
13
16
17
59
58
51
57
60
63
65
67
71
73
87
93
127
101
115
129
143
157
155
153
158
166
169
171
173
183
185
197
199

Fig. 4

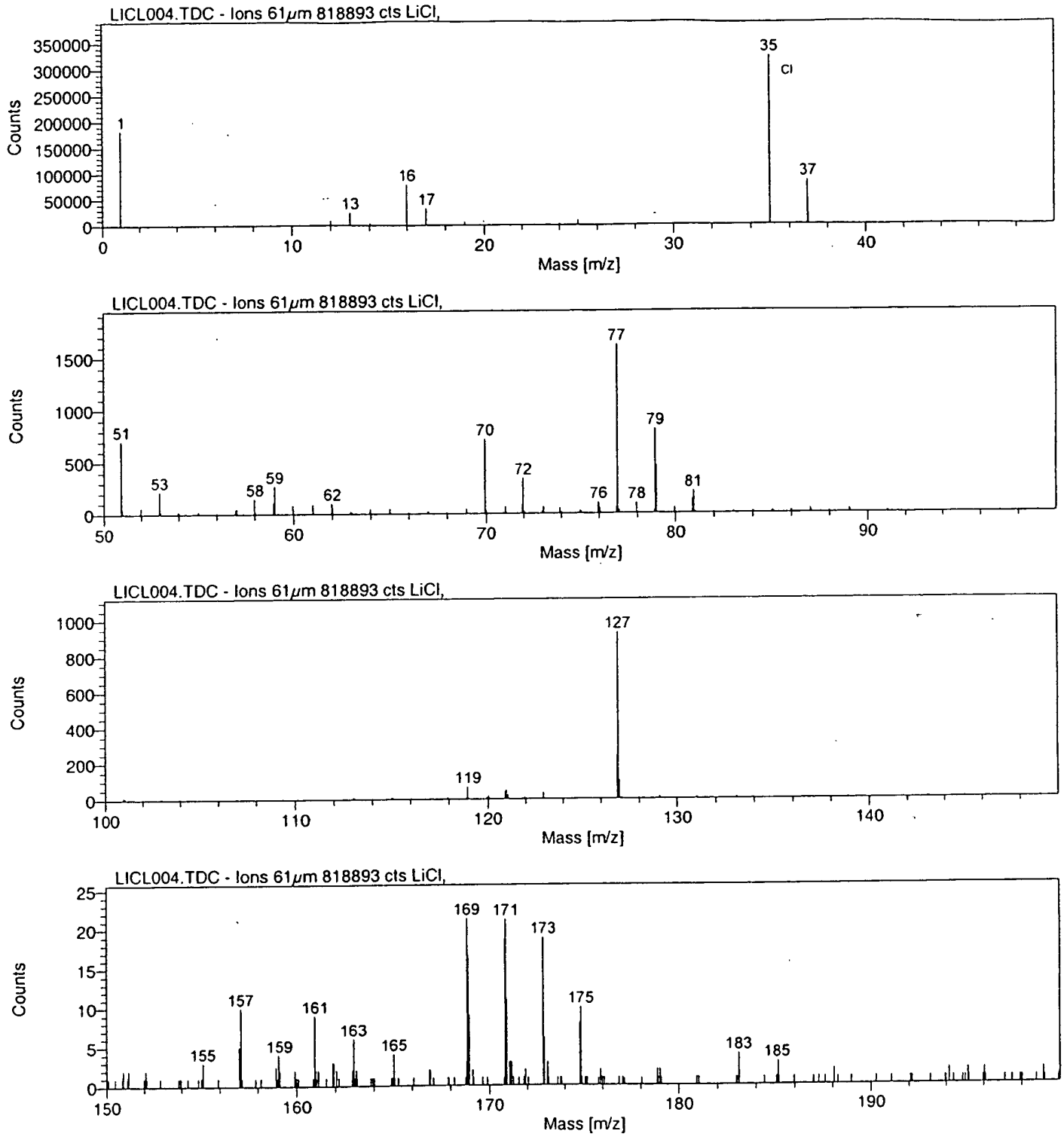
LICL004.TDC - Ions 61μm 818893 cts LiCl,
Counts
Mass [m/z]
35
Cl
37
1
16
17
13
LICL004.TDC - Ions 61μm 818893 cts LiCl,
77
79
70
72
51
53
58
59
62
76
78
81
LICL004.TDC - Ions 61μm 818893 cts LiCl,
127
119
LICL004.TDC - Ions 61μm 818893 cts LiCl,
169
171
173
157
161
175
163
155
159
165
183
185

Fig. 5

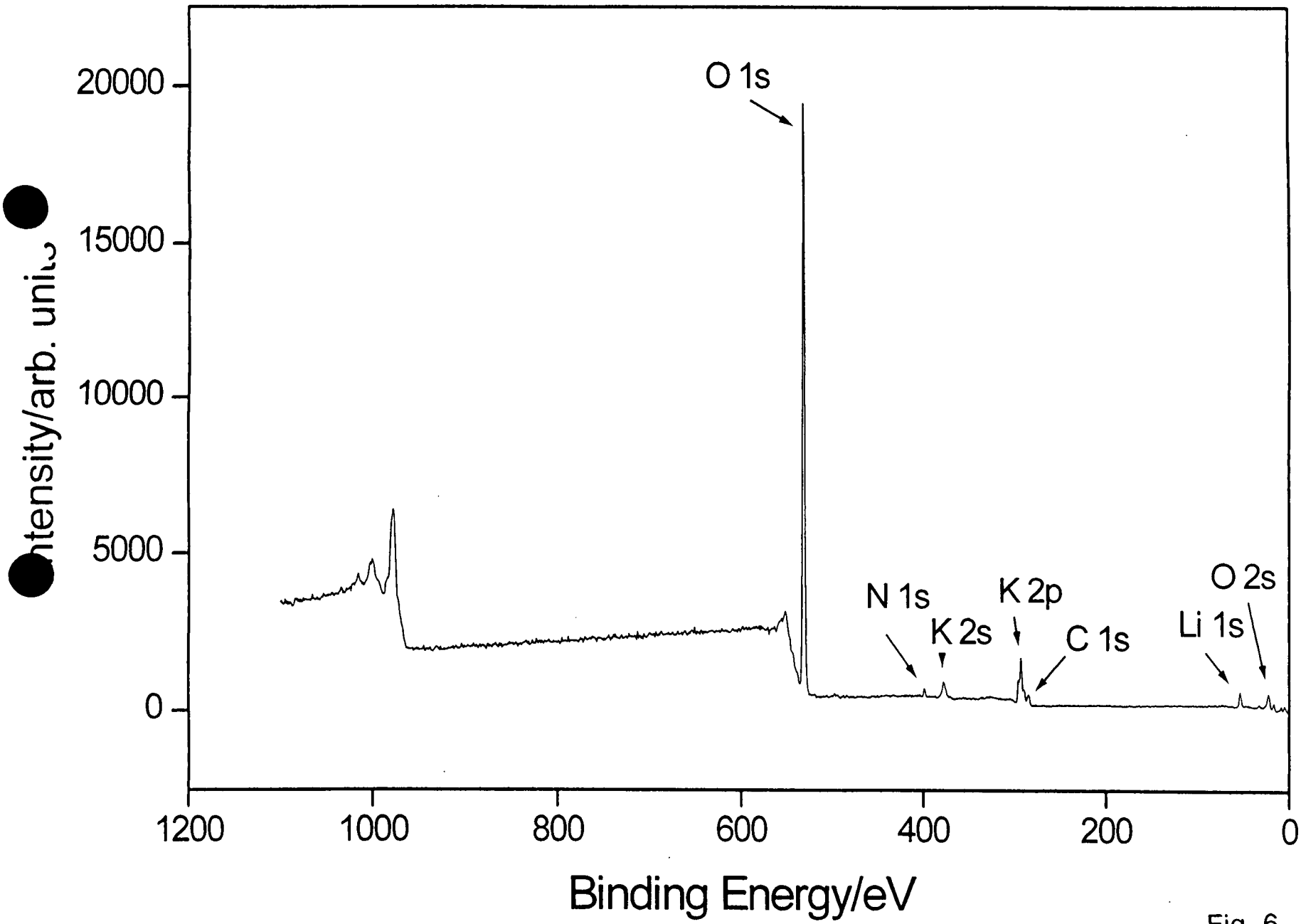
20000
15000
10000
5000
0
Intensity/arb. units
O 1s
N 1s
K 2s
K 2p
C 1s
Li 1s
O 2s
1200
1000
800
600
400
200
0
Binding Energy/eV

Fig. 6

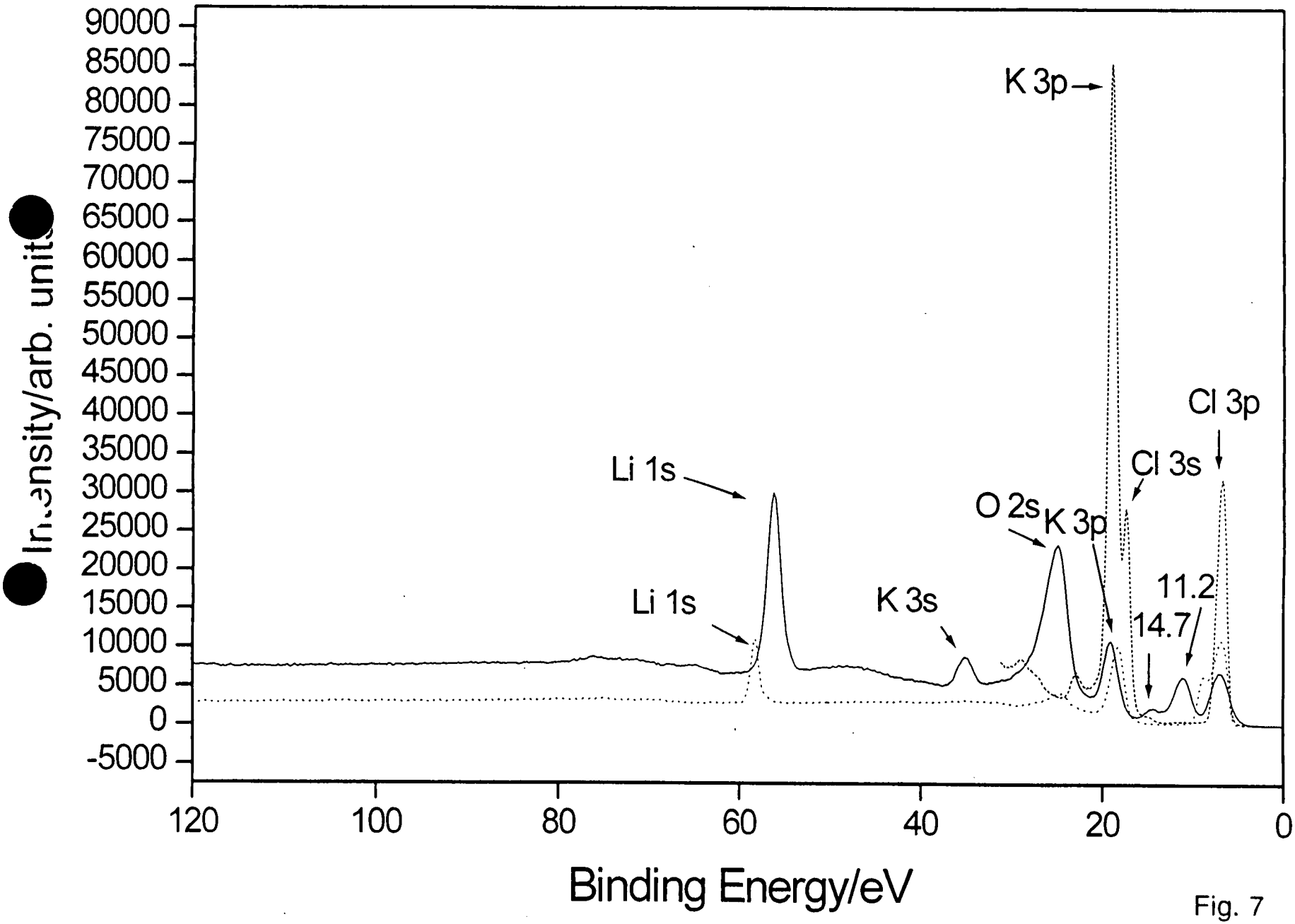
90000
85000
80000
75000
70000
65000
60000
55000
50000
45000
40000
35000
30000
25000
20000
15000
10000
5000
0
-5000
Intensity/arb. units
120
100
80
60
40
20
0
Binding Energy/eV
K 3p
Cl 3p
Cl 3s
Li 1s
O 2s
K 3p
Li 1s
K 3s
11.2
14.7

Fig. 7

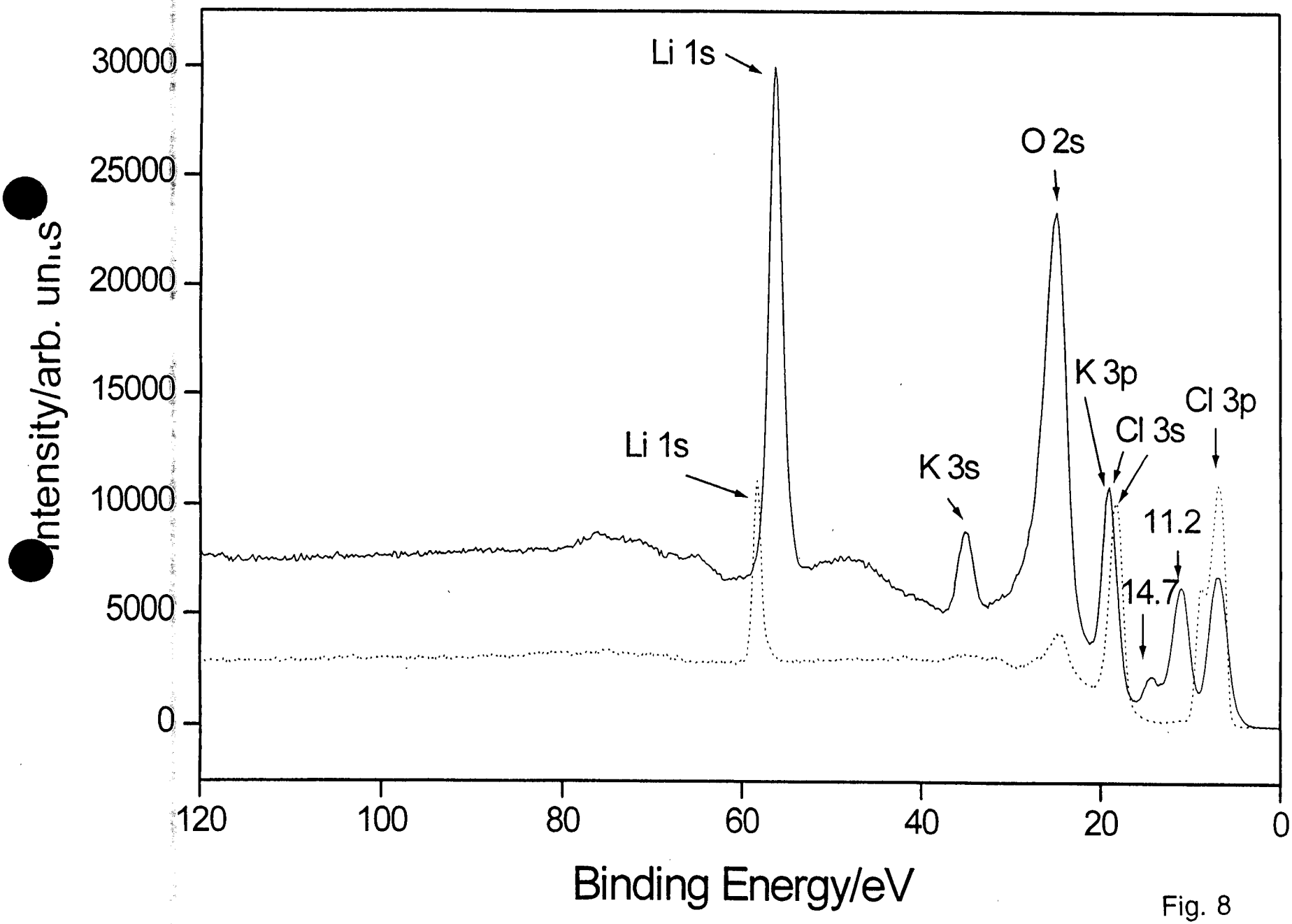
Intensity/arb. units
30000
25000
20000
15000
10000
5000
0
120
100
80
60
40
20
0
Binding Energy/eV
Li 1s
Li 1s
O 2s
K 3p
Cl 3s
Cl 3p
K 3s
11.2
14.7

Fig. 8

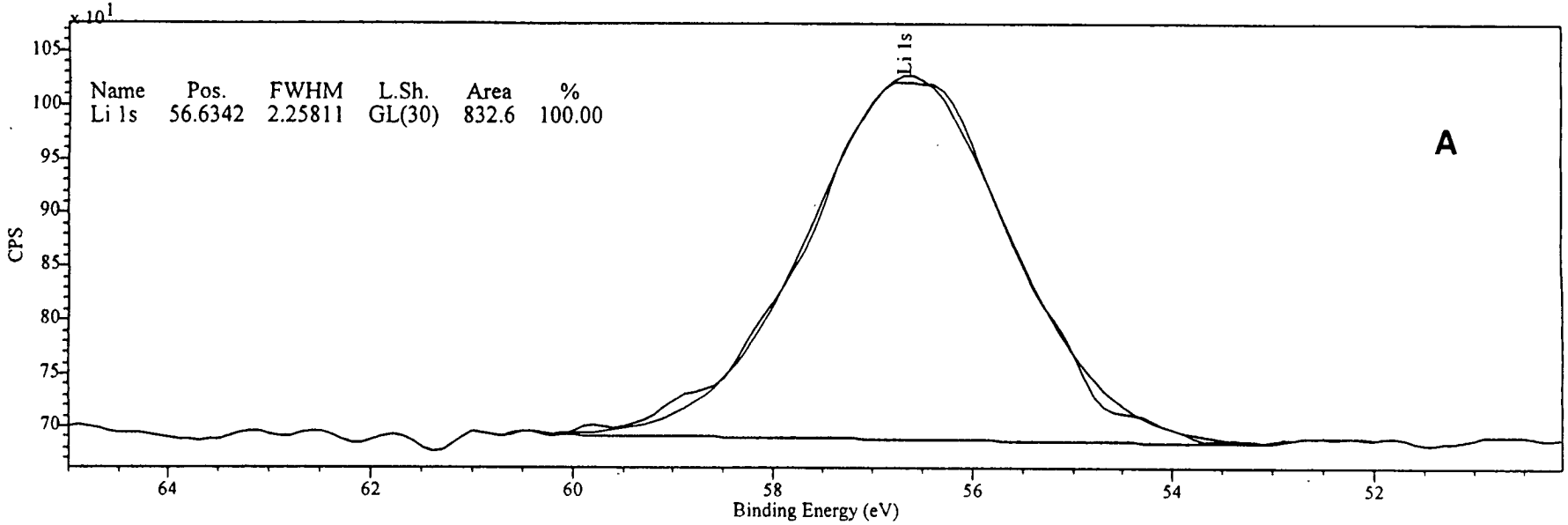
x 10^1
105
100
95
90
85
80
75
70
CPS
Name Pos. FWHM L.Sh. Area %
Li 1s 56.6342 2.25811 GL(30) 832.6 100.00
Li 1s
A
64
62
60
58
56
54
52
Binding Energy (eV)

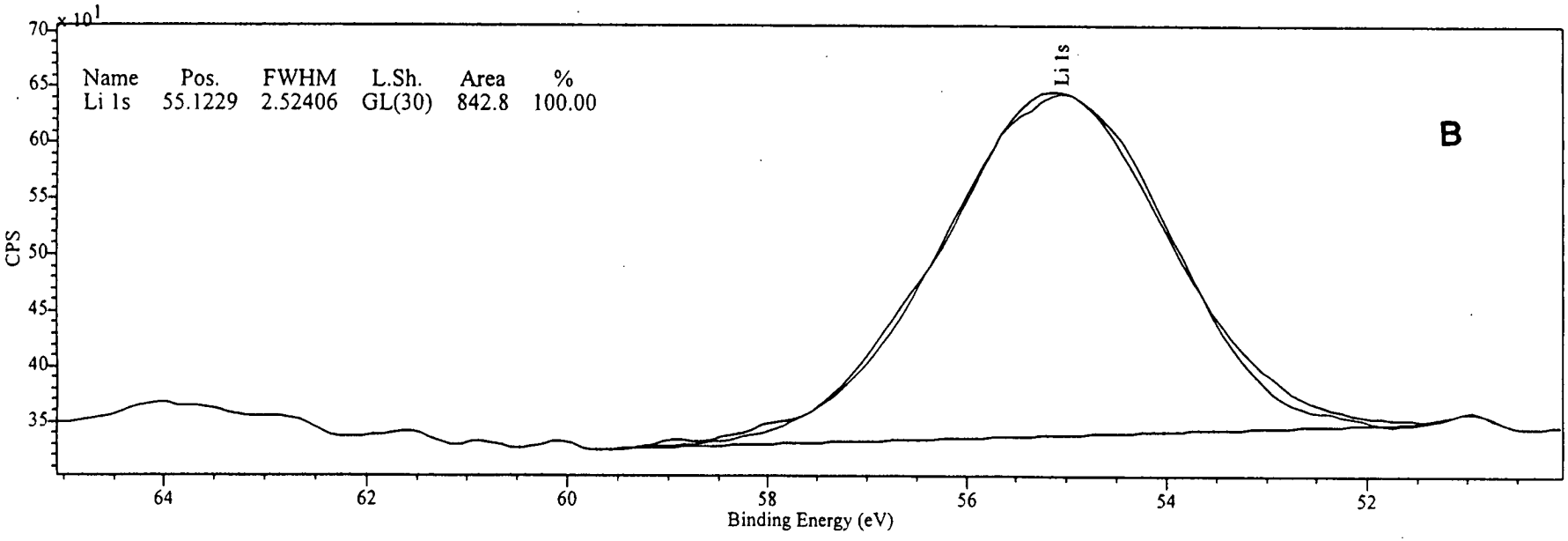
x 10^1
70
65
60
55
50
45
40
35
CPS
Name Pos. FWHM L.Sh. Area %
Li 1s 55.1229 2.52406 GL(30) 842.8 100.00
Li 1s
B
64
62
60
58
56
54
52
Binding Energy (eV)

Fig. 9

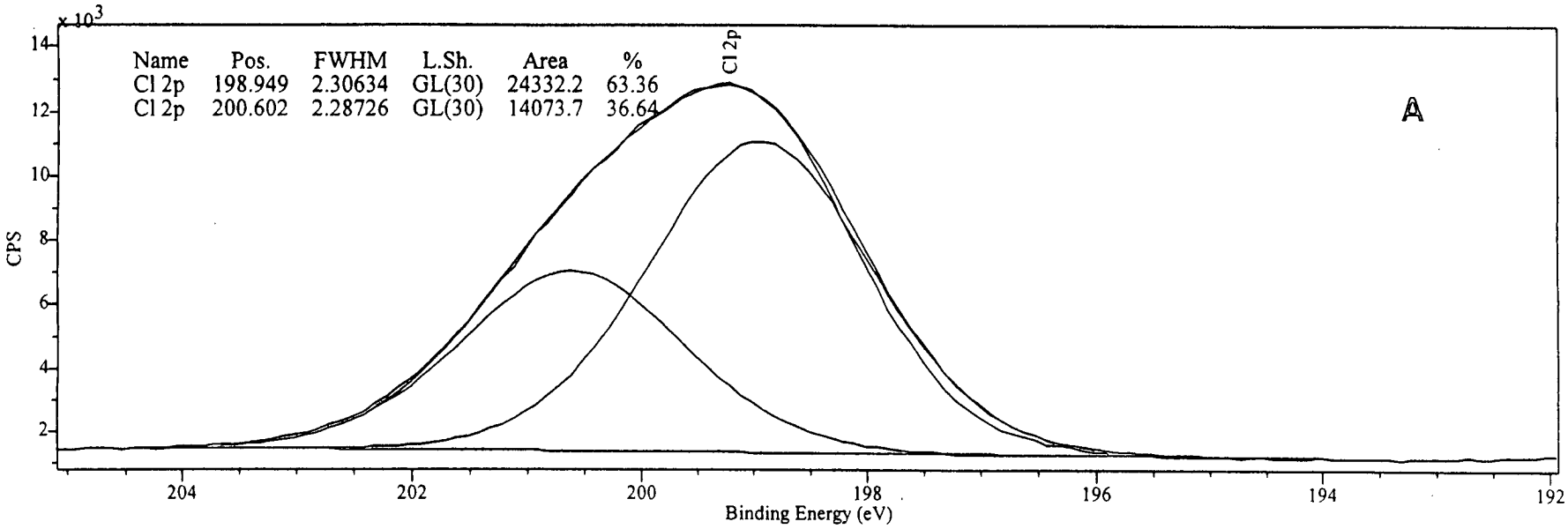
x 10^3
Name Pos. FWHM L.Sh. Area %
Cl 2p 198.949 2.30634 GL(30) 24332.2 63.36
Cl 2p 200.602 2.28726 GL(30) 14073.7 36.64
Cl 2p
A
CPS
Binding Energy (eV)

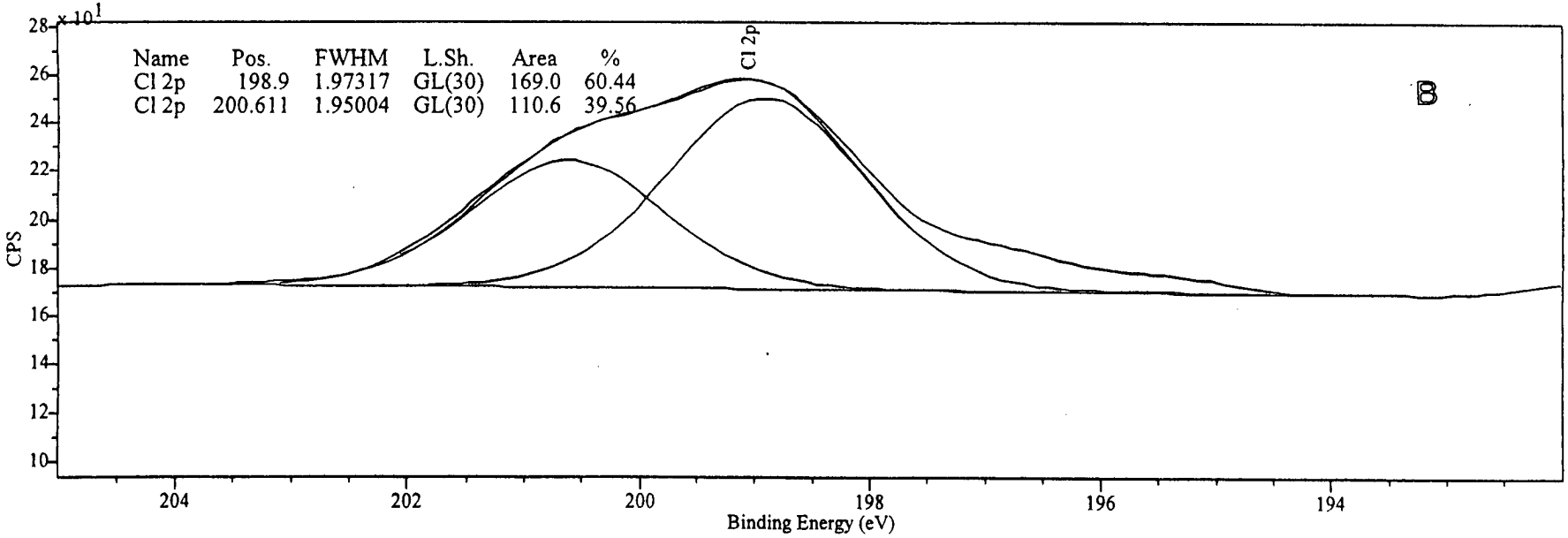
x 10^1
Name Pos. FWHM L.Sh. Area %
Cl 2p 198.9 1.97317 GL(30) 169.0 60.44
Cl 2p 200.611 1.95004 GL(30) 110.6 39.56
Cl 2p
B
CPS
Binding Energy (eV)

Fig. 10

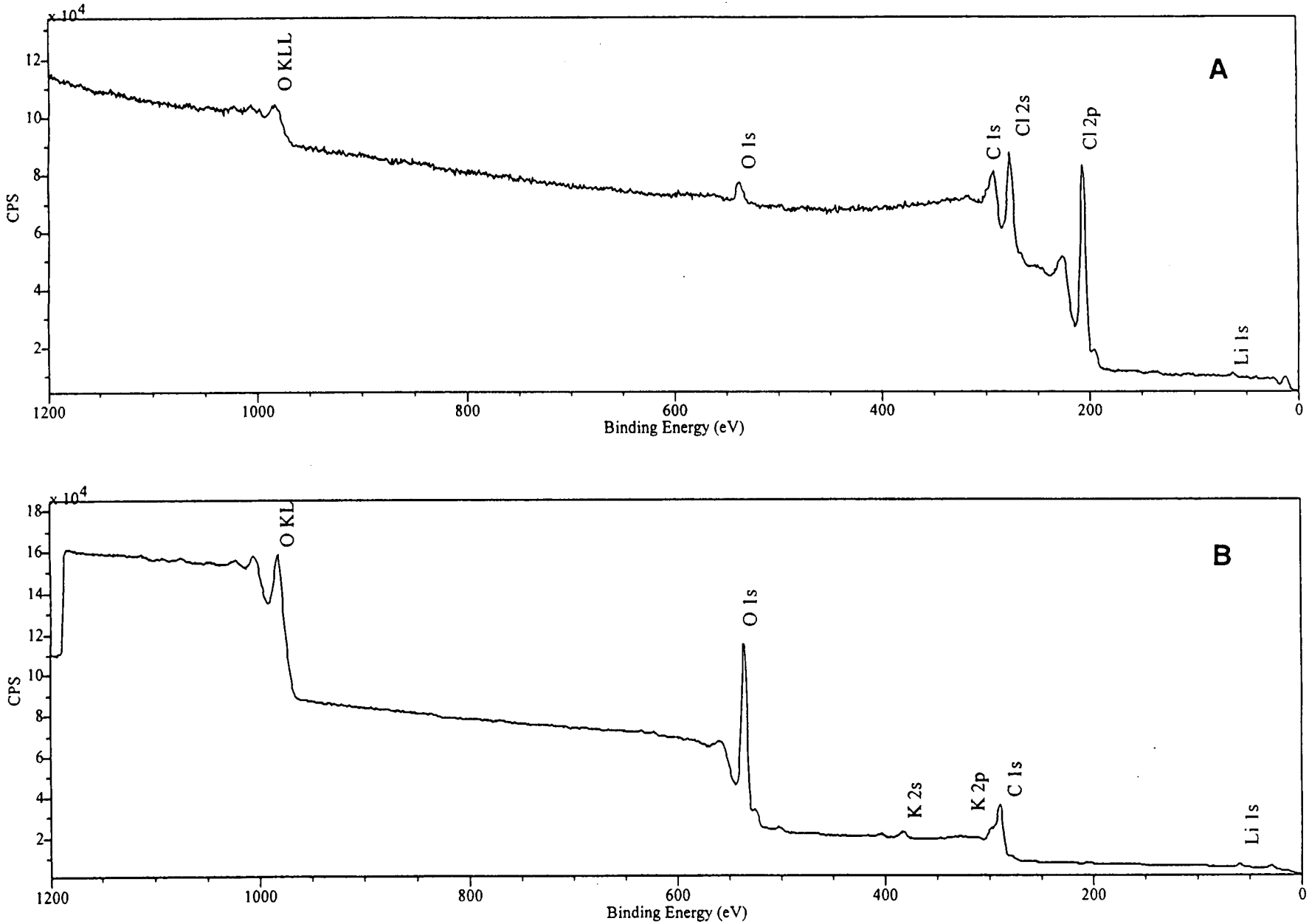
A
x 10^4
12
10
8
6
4
2
CPS
O KLL
O 1s
C 1s
Cl 2s
Cl 2p
Li 1s
1200
1000
800
600
400
200
0
Binding Energy (eV)
B
x 10^4
18
16
14
12
10
8
6
4
2
CPS
O KL
O 1s
K 2s
K 2p
C 1s
Li 1s
1200
1000
800
600
400
200
0
Binding Energy (eV)

Fig. 11

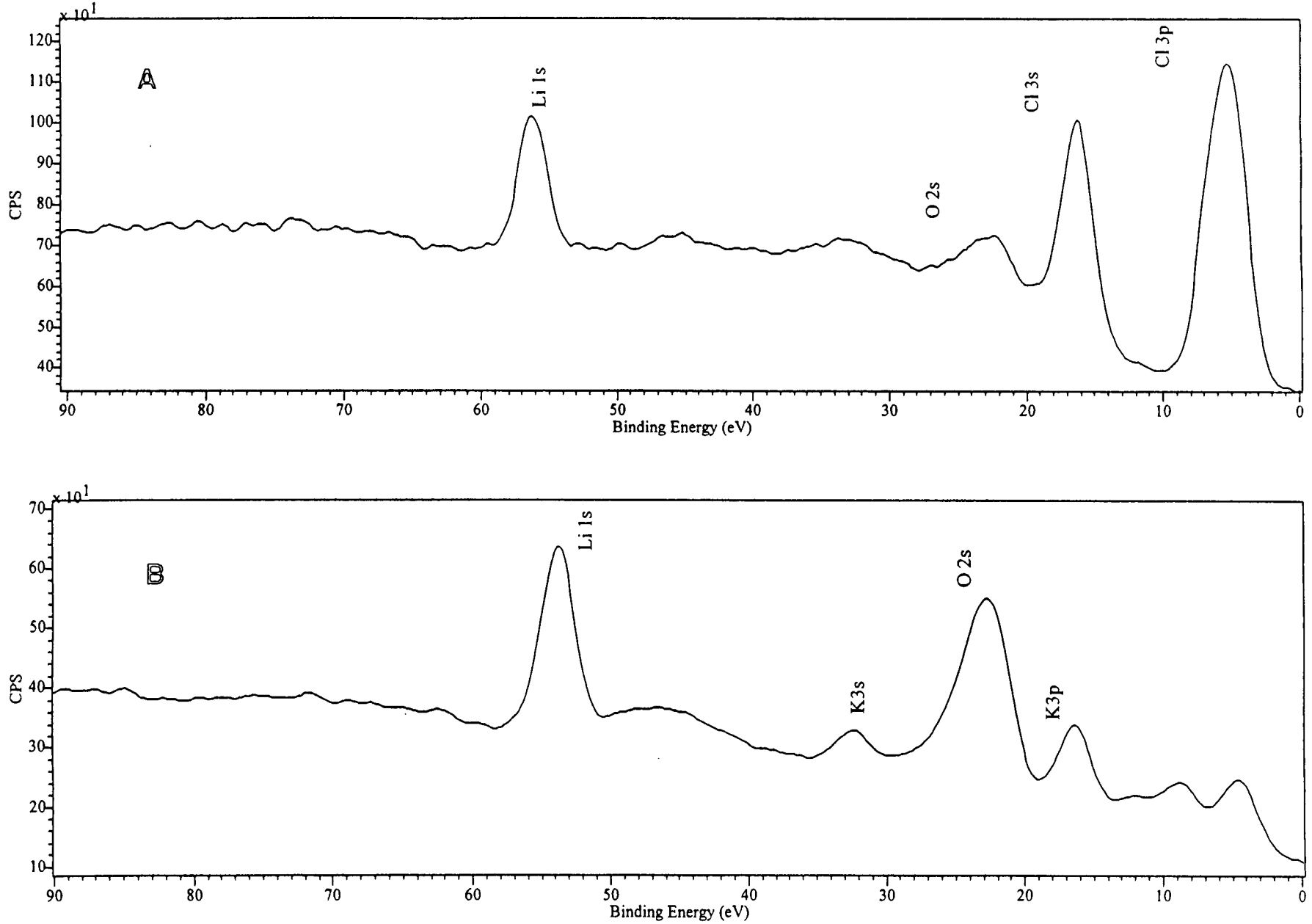
A
x 10^1
CPS
Li 1s
O 2s
Cl 3s
Cl 3p
Binding Energy (eV)
B
x 10^1
CPS
Li 1s
K3s
O 2s
K3p
Binding Energy (eV)

Fig. 12

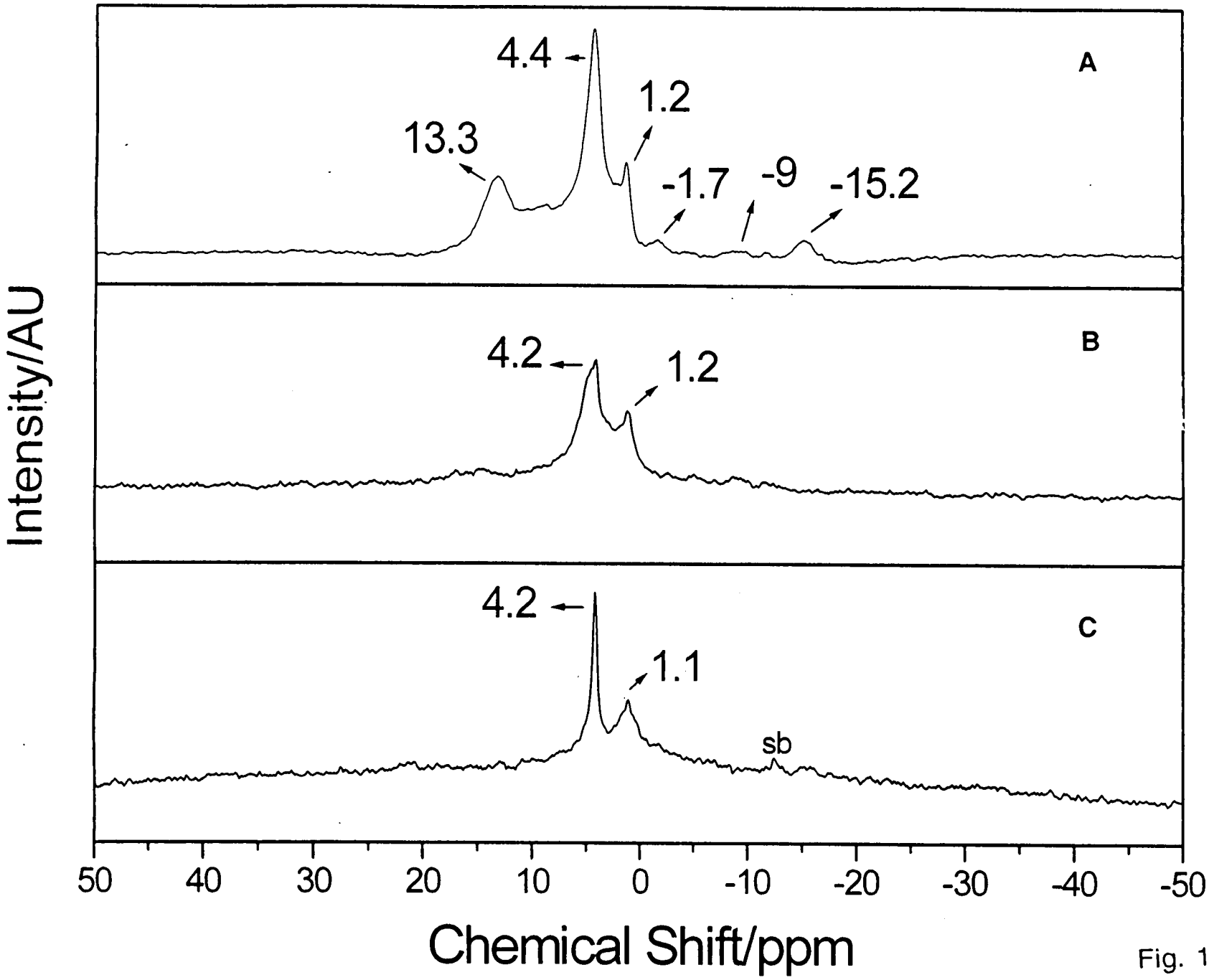
4.4
1.2
13.3
-1.7
-9
-15.2
A
4.2
1.2
B
4.2
1.1
sb
C
Intensity/AU
50
40
30
20
10
0
-10
-20
-30
-40
-50
Chemical Shift/ppm

Fig. 13

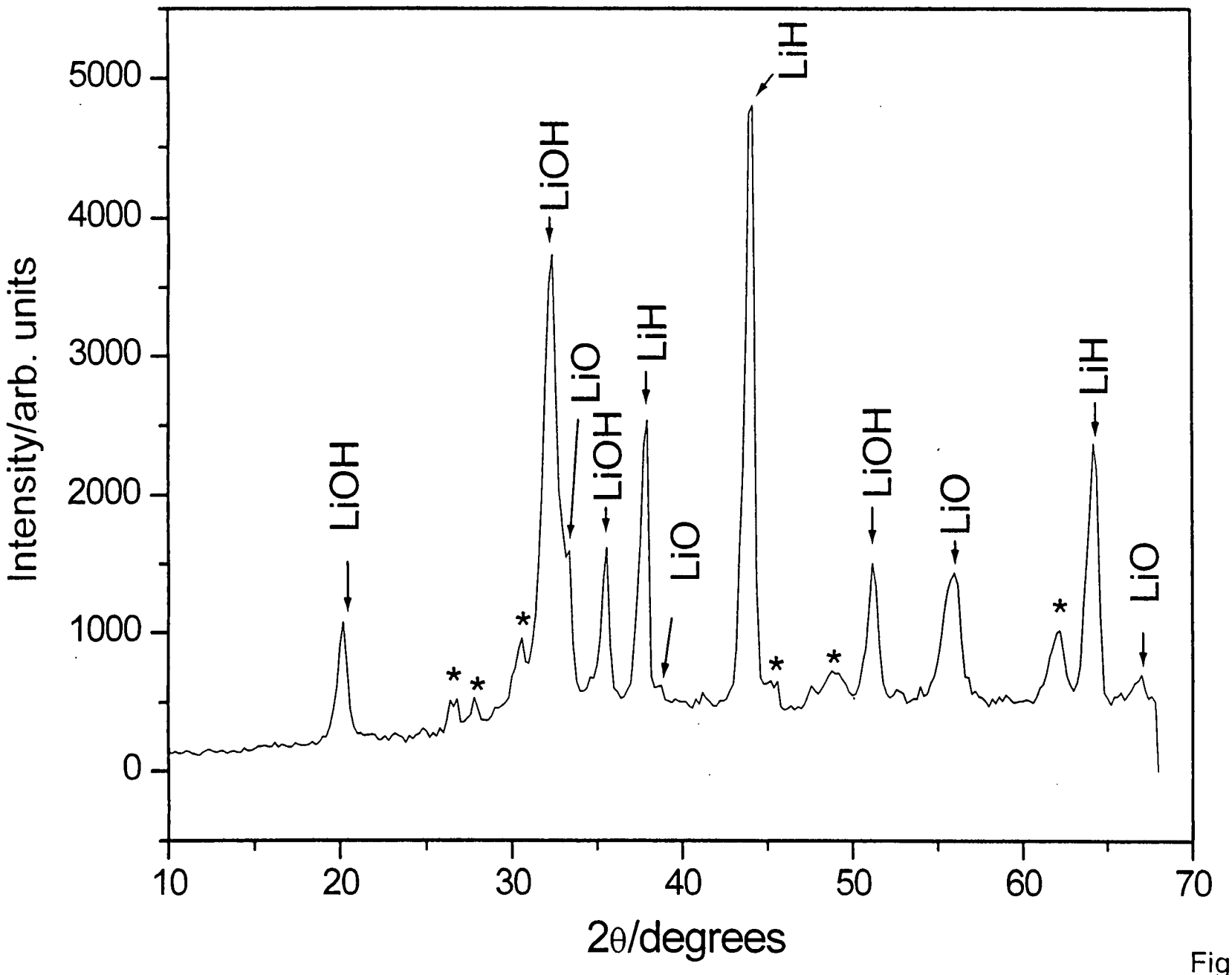
Intensity/arb. units
5000
4000
3000
2000
1000
0
10
20
30
40
50
60
70
2θ/degrees
LiOH
LiOH
LiO
LiOH
LiH
LiO
LiH
LiOH
LiO
LiH
LiO
*
*
*
*
*
*

Fig. 14